Received: 16 August 2019 | Revised: 20 November 2019 | Accepted: 12 December 2019

DOI: 10.1002/rcm.8699

Rapid Communications in Mass Spectrometry WILEY

SPECIAL ISSUE RESEARCH ARTICLE

Electrospray ionization tandem mass spectrometry of monoketone curcuminoids

Tatiana M. Vieira[1] | Renato P. Orenha[2] | Eduardo J. Crevelin[1] | Saulo S.P. Furtado[2] | Ricardo Vessecchi[1] | Renato L.T. Parreira[2] | Antônio E.M. Crotti[1]

[1]Departamento de Química, Faculdade de Filosofia, Ciências e Letras de Ribeirão Preto, Universidade de São Paulo, Av. Bandeirantes, 3900, Monte Alegre, CEP 14040-901Ribeirão Preto, SP, Brazil

[2]Núcleo de Pesquisas em Ciências Exatas e Tecnológicas, Universidade de Franca, CEP 14404-600Franca, SP, Brazil

Correspondence
A. E. M. Crotti, Departamento de Química, Faculdade de Filosofia, Ciências e Letras de Ribeirão Preto, Universidade de São Paulo, Av. Bandeirantes, 3900, Monte Alegre, CEP 14040-901, Ribeirão Preto, SP, Brazil.
Email: millercrotti@ffclrp.usp.br

Funding information
Conselho Nacional de Desenvolvimento Científico e Tecnológico, Grant/Award Number: 313648/2018-2; Coordenação de Aperfeiçoamento de Pessoal de Nível Superior, Grant/Award Number: Finance Code 001; Fundação de Amparo à Pesquisa do Estado de São Paulo, Grant/Award Numbers: 2011/07623-8, 2016/19272-9, 2017/24856-2

Rationale: Although monoketone curcuminoids (MKCs) have been largely investigated due to their biological activities, data on the gas-phase fragmentation reactions of protonated MKCs under collision-induced dissociation (CID) conditions are still scarce. Here, we combined electrospray ionization tandem mass spectrometry (ESI-MS/MS) data, multiple-stage mass spectrometry (MS^n), deuterium exchange experiments, accurate-mass data, and thermochemical data estimated by computational chemistry to elucidate and to rationalize the fragmentation pathways of eleven synthetic MKCs.

Methods: The MKCs were synthesized by Claisen-Schmidt condensation under basic (**1–9**) or acidic (**10–11**) conditions. ESI-CID-MS/MS analyses and deuterium-exchange experiments were carried out on a triple quadrupole mass spectrometer. MS^n analyses on an ion trap mass spectrometer helped to elucidate the fragmentation pathways. Accurate-mass data and thermochemical data, obtained at the B3LYP/6–31+G(d,p) level of theory, were used to support the ion structures.

Results: The most intense product ions were the benzyl ions ($[C_7H_2R_1R_2R_3R_4R_5]^+$) and the acylium ions ($[M + H - C_8H_3R_1R_2R_3R_4R_5]^+$), which originated directly from the precursor ion as a result of two competitive hydrogen rearrangements. Product ions $[M + H - H_2O]^+$ and $[M + H - C_6HR_1R_2R_3R_4R_5]^+$, which are formed after Nazarov cyclization, were also common to all the analyzed compounds. In addition, •Br and •Cl eliminations were diagnostic for the presence of these halogen atoms at the aromatic ring, whereas $•CH_3$ eliminations were useful to identify the methyl and methoxy groups attached to this same ring. Nazarov cyclization in the gas phase occurred for all the investigated MKCs and did not depend on the presence of the hydroxyl group at the aromatic ring. However, the presence and the position of a hydroxyl group at the aromatic rings played a key role in the Nazarov cyclization mechanism.

Conclusions: Our results reinforce some aspects of the fragmentation pathways previously published for 1,5-*bis*-(2-methoxyphenyl)-1,4-pentadien-3-one and 1,5-*bis*-(2-hydroxyphenyl)-1,4-pentadien-3-one. The alternative fragmentation mechanism proposed herein can explain the fragmentation of a wider diversity of monoketone curcuminoids.

1 | INTRODUCTION

Curcumin (1,7-*bis*(4-hydroxy-3-methoxyphenyl)-hepta-1,6-dien-3,5-dione], **I**, Figure 1) is a hydrophobic phenolic compound isolated from turmeric (*Curcuma* sp.).[1-3] The term "curcuminoids" is used to describe curcumin and other α,β-unsaturated *bis*-β-diketone analogues (e.g., demethoxycurcumin (**II**) and *bis*-demethoxycurcumin (**III**)) and structurally related compounds, such as monoketone curcuminoids (**IV**), 4-hydroxymethylene curcuminoids (**V**), and 4-arylidene curcuminoids (**VI**, Figure 1).

Monoketone curcuminoids (MKCs), also named mono-carbonyl curcuminoids, are 1,5-diaryl-penta-1,4-diene-3-ones. These compounds have attracted interest due to their structural similarity with curcumin (MKCs have one less methylene and one less carbonyl group than curcumin) and to their various biological activities, including antimicrobial,[4] cytotoxic,[2] anti-inflammatory,[1] antiparasitic,[5] and anti-HIV actions.[6]

Over the last decade, electrospray ionization tandem mass spectrometry (ESI-MS/MS) has been used to identify natural and synthetic organic compounds mainly in combination with liquid chromatography (LC/MS/MS). Because MS is highly sensitive, it has been widely employed in *in vitro* and *in vivo* metabolism studies.[7] In this context, the MS/MS data of the class of compounds under study play a key role.[8] The gas-phase fragmentation reactions of a series of protonated and deprotonated β-diketone curcuminoids have been previously investigated.[9,10] However, in the case of the MKCs, data on their fragmentation are still scarce. To date, a systematic study of only three compounds has been performed by Cyriac and co-workers, who proposed the occurrence of a Nazarov cyclization to explain the eliminations of anisole and/or ketene from protonated 1,5-*bis*-(2-methoxyphenyl)-1,4-pentadien-3-one and 1,5-*bis*-(2-hydroxyphenyl)-1,4-pentadien-3-one.[11] In solution, the Nazarov cyclization is an acid-catalyzed cyclization reaction of divinyl ketones to cyclopentanones. The mechanism involves the conrotatory electrocyclic ring closure of a protonated divinyl ketone followed by deprotonation and double-bond reorganization.[12] In solution, sufficiently basic substituents like OCH_3 or OH in the *ortho* position may cause deprotonation during Nazarov cyclization or aid proton transfer. This reaction has aroused great interest in mass spectrometry because these groups can catalyze proton migration in the gas phase.[12] George and co-workers have shown that Nazarov cyclization of protonated chalcones in the gas phase is analogous to Nazarov cyclization in solution, but its occurrence in the gas phase depends on the employed protonation method and the nature and position of the substituents at the aromatic ring. More recently, Cyriac and co-workers also verified that the gas-phase Nazarov cyclization of protonated 2-methoxychalcone is analogous to the corresponding process in solution. The authors extended their studies to 1,5-*bis*- (2-methoxyphenyl)-1,4-pentadien-3-one to demonstrate that the methoxy group acts as an effective "catalyst" for the transfer of protons involved in the cyclization step.[11]

As part of our ongoing project on the gas-phase fragmentation reactions of biologically active synthetic and natural compounds,[13-21] and given the scarcity of ESI-MS/MS data of MKCs, here we investigate the gas-phase fragmentation pathways of selected curcuminoids by ESI-MS/MS combined with thermochemical data obtained at the B3LYP/6-31+G(d) level of theory.

2 | EXPERIMENTAL

2.1 | Synthesis of monoketone curcuminoids 1–11

Compounds **1–9** were obtained by aldol condensation between acetone and different aromatic aldehydes according to a previously published methodology (Scheme 1).[4] Briefly, a solution of NaOH (2.5 mol/L) and ethanol (20 mL) was added to a flask (100- mL) containing an aromatic aldehyde (26 mmol) and acetone (0.95 mL, 13 mmol). The reaction mixture was stirred at 0°C for 1–24 h, washed with cold water (to remove the excess base), and filtered under reduced pressure. The resulting solids were dried under vacuum, to yield compounds **1** (24% yield), **2** (64% yield), **3** (69% yield), **4** (83% yield), **5** (20% yield), **6** (72% yield), **7** (45% yield), **8** (97% yield), and **9** (44% yield). Compounds **10** and **11** were synthesized by Claisen-Schmidt condensation in acidic conditions according to the methodology described in the literature.[6] Initially, acetic acid (50 mL) was saturated with hydrogen chloride at 0°C. Next, a mixture of vanillin (3.95 g, 26 mmol) and acetone (0.75 g, 13 mmol) was slowly added to the acid. The mixture was brought to room temperature and stirred for 24 h. Subsequently, the crude mixture was poured into ice-cold water (200 mL) and extracted with ethyl acetate (3 × 30 mL); the organic phase was dried over $MgSO_4$. After the solvent had been

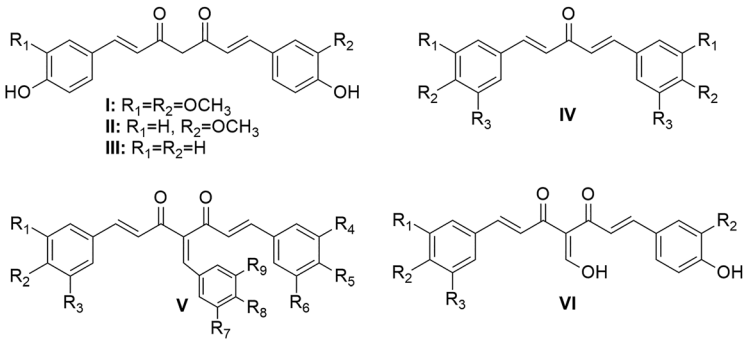

FIGURE 1 Chemical structures of curcumin (**I**), demethoxycurcumin (**II**), *bis*-demethoxycurcumin (**III**), and structurally related monoketone curcuminoids (**IV**), 4-hydroxymethylene curcuminoids (**V**), and 4-arylidene curcuminoids (**IV**)

SCHEME 1 Synthesis of monoketone curcuminoids **1–11**

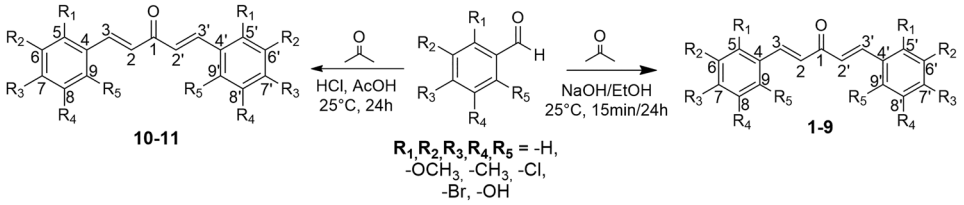

	1	2	3	4	5	6	7	8	9	10	11
R_1	H	H	H	H	H	H	H	OMe	H	H	H
R_2	H	H	H	H	H	OMe	H	H	H	H	H
R_3	H	OMe	Me	OMe	H	OMe	Br	OMe	Cl	OH	OH
R_4	H	H	H	OMe	H	OMe	H	H	H	OMe	H
R_5	H	H	H	H	Cl	H	H	OMe	H	H	H

removed by evaporation under reduced pressure in a rotary evaporator, the resulting mixture was purified by flash column chromatography; isocratic elution with hexane/ethyl acetate 1:1 (v/v) was employed. Finally, compounds **10** and **11** (21% and 44% yield, respectively) were obtained as yellow solids. All the compounds were identified on the basis of their ^{1}H and ^{13}C NMR, ESI-MS, UV and IR data (see supporting information).

2.2 | Mass spectrometry analyses

Electrospray ionization tandem mass spectrometry (ESI-MS/MS) analyses of curcuminoids **1–11** were carried out on a Xevo TQS tandem quadrupole mass spectrometer (QqQ; Waters, Milford, MA, USA) equipped with a Z-spray ionization source operating in the positive ion mode. The samples were dissolved in MeOH/H_2O 4:1 (v/v) to achieve a final concentration of curcuminoids of 1.0 μg/mL. Next, traces of 0.1% formic acid were added, and the sample was infused directly into the ionization source at a flow rate of 0.1 mL/min. In the case of deuterium-exchange experiments, compounds **1–11** were dissolved in MeOH/D_2O 1:1 (v/v). To maximize the relative intensity of the peaks corresponding to the protonated MKCs, the capillary and the cone voltages were optimized to 3.2 kV and 40 V, respectively. Electrospray ionization collision-induced dissociation tandem mass spectrometry (ESI-CID-MS/MS) experiments were carried out by using argon (99.999% purity) as the collision gas on the selected precursor ion ($[M + H]^+$) at collision energy values ranging from 5 to 50 eV. The ionization source temperature was 150°C and the desolvation gas temperature (N_2) was 250°C. The injected sample volume was 5 μL.

Multiple-stage ESI mass spectrometry ($ESI\text{-}MS^n$) analyses were performed on an ion trap (IT) mass spectrometer (Amazon Speed, Bruker Daltonics, Bremen, Germany) operating in the positive ion mode. The ion trap amplitude was varied from 40 to 60 and optimized for each compound. N_2 was used as nebulizing (6 psi pressure) and drying gas (8 mL/min flow rate, 220°C temperature), and the capillary voltage and the end plate offset voltage were set to 3.5 kV and 500 V, respectively. The analytical mass range was *m/z* 50–450.

2.3 | Computational methods

The geometry of all the structures was optimized by the B3LYP computational method[22,23] and the 6-31+G(d,p)[24] basis set with Gaussian09 software.[25] The vibrational frequency analysis demonstrated that all the studied compounds were in a minimum on their respective potential energy surfaces. The Gibbs energies and the enthalpies calculated at 298.15 K of the most stable ion structures were used to investigate the fragmentation pathways. The gas-phase proton affinity (PA) values were calculated from the protonation reaction Gibbs energy and enthalpy: $M + H^+ \rightarrow MH^+$, as has usually been done in recent studies.[15,23] The experimental enthalpy and the Gibbs energy values that were considered for the proton were 1.48 and −6.28 kcal mol^{-1}, respectively.[22]

3 | RESULTS AND DISCUSSION

3.1 | Structure–fragmentation correlations

When a series of compounds that share the same structural core is available, comparison between their product ion spectra obtained at an optimum collision energy (E_{lab}) can provide useful structural fragmentation correlations to elucidate their gas-phase fragmentation pathways.[13,15] The optimum value of E_{lab} is usually expected to reduce the relative intensity of the protonated molecule in the product ion spectrum to below 50% without promoting extensive fragmentation. Thus, on the basis of the relative intensity (RI, %) versus E_{lab} (eV) plots, the optimum E_{lab} for MKCs **1–11** was 20 eV (Figure 2 for compound **1**, and supporting information for compounds **2–11**).

Figure 3 shows the product ion spectra of the protonated compounds obtained at E_{lab} = 20 eV; Table 1 summarizes their main product ions (relative intensity higher than 5%), where **H** is the most intense product ion in the spectra of most of the analyzed compounds. This ion results from direct elimination of $C_{10}H_4OR_1R_2R_3R_4R_5$ from the protonated molecule (**A**). Formation of **D** from **A** by elimination of $C_8H_3OR_1R_2R_3R_4R_5$ competes with formation of **H**, as shown in Scheme 2. Other common product ions

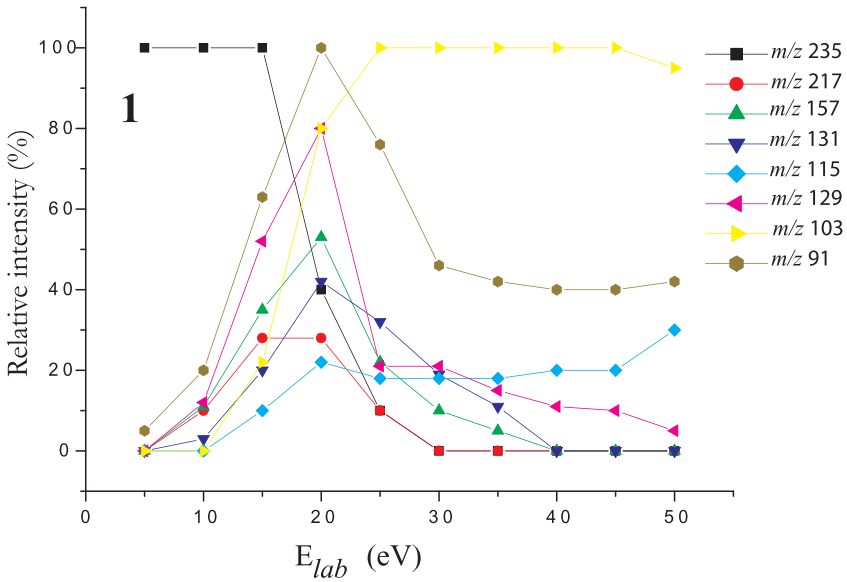

FIGURE 2 Correlation between the relative intensity (%) and the collision energy (E_{lab}, in eV) for compound **1** [Color figure can be viewed at wileyonlinelibrary.com]

include **B** (**A**–H_2O), **C** (**A**–$C_6HR_1R_2R_3R_4R_5$), and **G** (**D**–CO). **F** (**C**–C_2H_2O) and **E** (**C**–CO) also appear in the spectra of most of the investigated MKCs, except for compound **7**. The MS^3 spectra support formation of **E** and **F** from **C** (see supporting information).

A detailed analysis of the product ion spectra of protonated compounds **1–11** allowed us to identify some diagnostic ions that could help to distinguish the nature of the substituents at the aromatic ring of these compounds (Scheme 2). Consecutive eliminations of two methyl radicals (15 Da each) from **B** to produce **Q** (*m/z* 230) and **R** (*m/z* 215) are diagnostic for compound **3**, which displays a methyl group at the aromatic ring. Similarly, formation of **T** (*m/z* 250 for compounds **5** and **9** and *m/z* 294 for compound **7**) from **B** and formation of **V** (*m/z* 215) from **T** due to radical X• eliminations (a chlorine for compounds **5** and **9** and a bromine for compound **7**) are diagnostic for compounds **5**, **7**, and **9**. Radical X• eliminations can also occur directly from **A**, to produce **S** (*m/z* 268 and *m/z* 312) and **U** (*m/z* 233), or from **G**, to form **P** (*m/z* 102). These eliminations are diagnostic for compounds **5**, **7**, and **9**. Methyl radical eliminations from other product ions also occur and produce product ions that are diagnostic for the methoxy group at the aromatic ring and specific for each compound. For example, •CH_3 elimination from **H**, **G**, **D**, and **E** yields **O** (*m/z* 136 for compound **4** and *m/z* 166 for compound **6**), **K** (*m/z* 206 for compounds **6** and **8**), **J** (*m/z* 118 for compound **2** and *m/z* 148 for compound **4**), and **Y** (*m/z* 160 for compound **10**), respectively, which are diagnostic for compounds **2**, **4**, **6**, **8**, and **10**. The MS^3 and MS^4 experiments also support formation of **J**, **K**, **L**, **O**, **Q**, **R**, **S**, **T**, **U**, and **V** (see supporting information).

3.2 | Protonation sites and gas-phase reactivity

The importance of determining the protonation site in gas-phase fragmentation studies under CID conditions has recently been discussed.[14,15]. In general, two possibilities are considered. The first, known as the "mobile proton theory",[24] assumes that the proton initially binds to the most basic site of the molecule and then migrates to more basic sites under CID conditions, with fragmentation occurring from species resulting from this migration. The second assumes that the proton remains bound to the most basic site of the molecule in the post-collision state. In this case, the translational energy is converted into internal energy, which triggers the fragmentation reactions.[26]

Figure 4 displays the proton affinity (PA) values for different sites of the structures of compounds **1–11**, as estimated by computational chemistry. These data indicate that the carbonyl oxygen is the most susceptible site to protonation for all the investigated MKCs, as previously reported by Cyriac and co-workers for compounds **1** and **2**.[11] Recently, Hu and co-workers studied the reactions of α,β-unsaturated aromatic ketones (chalcones) during mass spectrometry. As in the case of MKCs, the investigated chalcones bear a vinyl unit between the carbonyl and the phenyl groups. The authors showed that the carbonyl oxygen in the studied chalcones is the most susceptible site to protonation; however, protonation at the carbon α to the carbonyl may also occur. The authors described proton migration from the carbonyl oxygen to less favorable sites, such as the α-carbon, as an energy-dependent process involving a certain energy barrier.[25] In the present study, we only consider the species protonated at the carbonyl oxygen as the precursor ion.

3.3 | Formation of product ions B–G

H (**A** – $C_{10}H_4OR_1R_2R_3R_4R_5$) and **D** (**A** – $C_8H_3OR_1R_2R_3R_4R_5$) are the most intense product ions in almost all the spectra of compounds **1–11** (Figure 3, Table 1). These ions originate directly from the precursor ion (protonated molecule) by two competitive hydrogen rearrangements, as depicted in Scheme 3. Formation of acylium ion

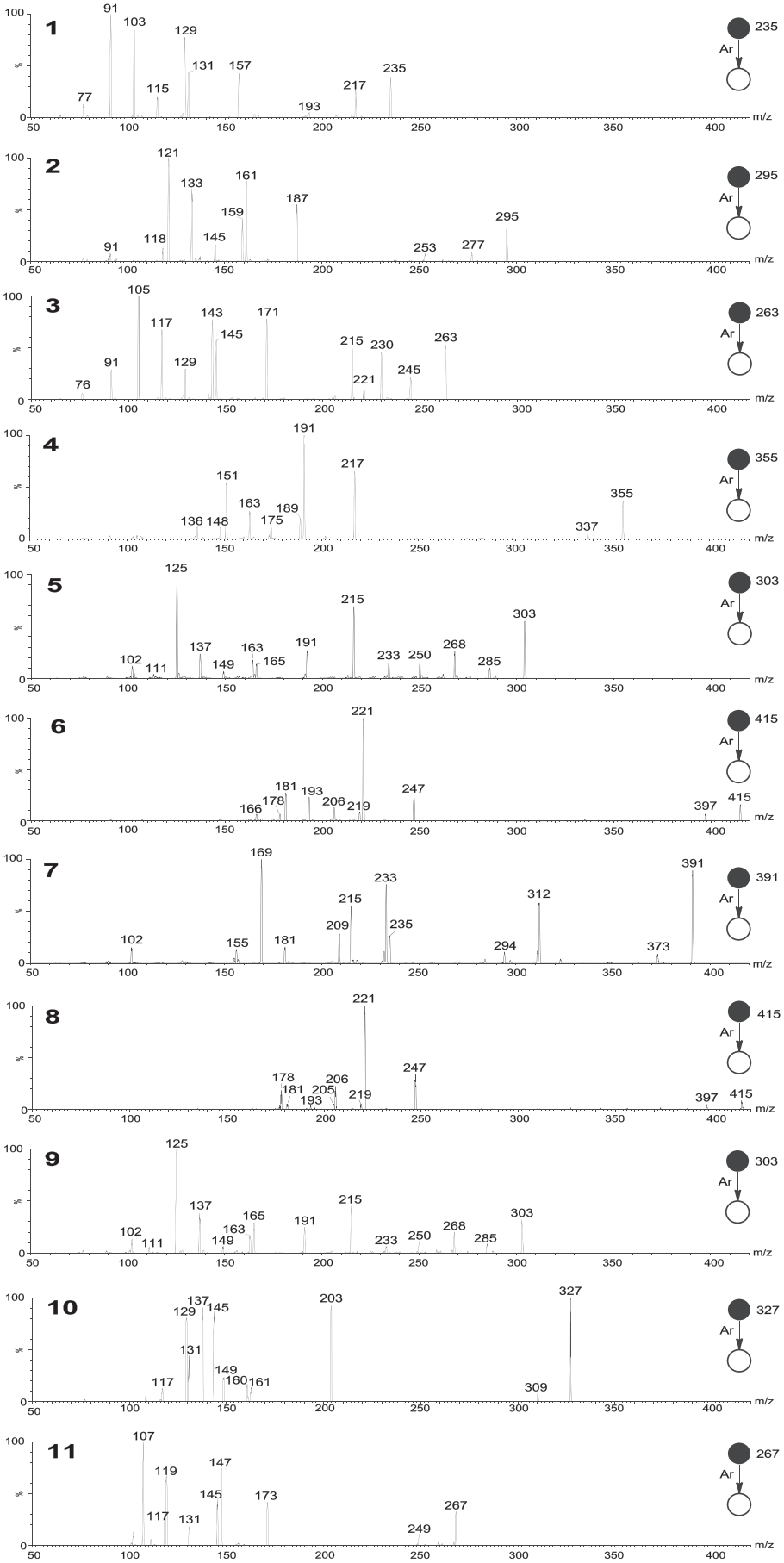

FIGURE 3 Product ion spectra of protonated monoketone curcuminoids **1–11** (QqQ, Ar, E_{lab} = 20 eV)

TABLE 1 Main product ions of protonated MKCs **1–11** at collision energy (E_{lab}) of 20 eV*

Assignment	1	2	3	4	5	6	7	8	9	10	11
A ($[M + H]^+$)	235 (40) *236*	295 (36) *296*	263 (62) *264*	355 (38) *356*	303 (56) *305*	415 (15) *416*	391 (90) *392*	415 (9) *416*	303 (42) *304*	327 (100) *328*	267 (36) *268*
B (**A**–H_2O)	217 (28) *217*	277 (9) *277*	245 (23) *245*	337 (7) *337*	285 (10) *285*	397 (5) *397*	373 (9) *373*	397 (5) *397*	285 (9) *285*	309 (9) *309*	249 (7) *249*
Q (**B**–•CH_3)	–	–	230 (50) *230*	–	–	–	–	–	–	–	–
R (**Q**–•CH_3)	–	–	215 (55) *215*	–	–	–	–	–	–	–	–
S (**A**–•X)	–	–	–	–	268 (12) *268*	–	312 (59) *312*	–	268 (20) *268*	–	–
X (**A**–C_2H_2O)	193 (5) *193*	253 (10) *253*	221 (14) *221*	–	–	–	–	–	–	–	–
T (**B**–•X)	–	–	–	–	250 (16) *250*	–	294 (11) *294*	–	250 (10) *250*	–	–
U (**S**–•X)	–	–	–	–	233 (15) *233*	–	233 (72) *233*	–	233 (5) *233*	–	–
V (**T**–•X)	–	–	–	–	215 (69) *215*	–	215 (55) *215*	–	215 (42) *215*	–	–
Y (**E**–•CH_3)	–	–	–	–	–	–	–	–	–	160 (13) *160*	–
C (**A**–$C_6HR_1R_2R_3R_4R_5$)	157 (53) *157*	187 (56) *187*	171 (88) *171*	217 (65) *217*	191 (27) *191*	247 (22) *247*	235 (25) *235*	247 (33) *247*	191 (25) *191*	203 (98) *203*	173 (43) *173*
D (**A**–$C_8H_3R_1R_2R_3R_4R_5$)	131 (42) *131*	161 (78) *161*	145 (62) *145*	191 (100) *191*	165 (14) *165*	221 (100) *221*	209 (30) *209*	221 (100) *221*	165 (30) *165*	131 (42) *131*	147 (77) *147*
E (**C**–CO)	129(80) *129*	159 (42) *159*	143 (85) *143*	189 (20) *189*	163 (18) *163*	219 (8) *219*	–	219 (5) *219*	163 (16) *163*	129(80) *129*	145 (45) *145*
F (**C**–C_2H_2O)	115 (22) *115*	145 (15) *145*	129 (32) *129*	175 (10) *175*	149 (5) *149*	205 (5) *205*	–	205 (15) *205*	149 (5) *149*	161 (12) *161*	131 (15) *131*
G (**D**–CO)	103 (80) *103*	133 (72) *133*	117 (73) *117*	163 (28) *163*	137 (21) *137*	193 (18) *193*	181 (15) *181*	193 (5) *193*	137 (35) *137*	149 (23) *149*	119 (61) *119*
H (**A**–$C_{10}H_8O$)	91 (100) *91*	121 (100) *121*	105 (100) *105*	151 (62) *151*	125 (100) *125*	181 (28) *181*	169 (100) *169*	181 (7) *181*	125 (100) *125*	137 (98) *137*	107 (100) *107*
W (**D**–CH_3OH)	–	–	–	–	–	–	–	–	–	145 (85)	–

(Continues)

TABLE 1 (Continued)

Assignment	1	2	3	4	5	6	7	8	9	10	11
										145	
Z (Z_1–CO)	–	–	–	–	–	–	–	–	–	117 (13)	117 (25)
										117	*117*
J (**G**–•CH_3)	–	118 (12)	–	148 (10)	–	–	–	–	–	–	–
		118		*148*							
O (**H**–•CH_3)	–	–	–	136 (12)	–	166 (5)	–	–	–	–	–
				136		*166*					
K (**D**–•CH_3)	–	–	–	–	–	206 (12)	–	206 (20)	–	–	–
						206		*206*			
I (**K**–CO)	–	–	–	–	–	178 (5)	–	178 (17)	–	–	–
						178		*178*			
P (**G**–•X)	–	–	–	–	102 (13)	–	102 (15)	–	102 (12)	–	–
					102		*102*		*102*		
L (**H**–CH_2O)	–	91 (8)	–	–	–	–	–	–	–	–	–
		91									
M (**D**–C_2H_2/-CO)	77 (12)	–	91 (32)	–	111 (5)	–	155 (10)	–	111 (5)	–	–
	77		*91*		*111*		*155*		*111*		
N (**H**–•CH_3)	–	–	76 (5)	–	–	–	–	–	–	–	–
			76								

*Relative intensities (%) are given in parentheses. Data from the deuterium-exchange experiments are given in italics.

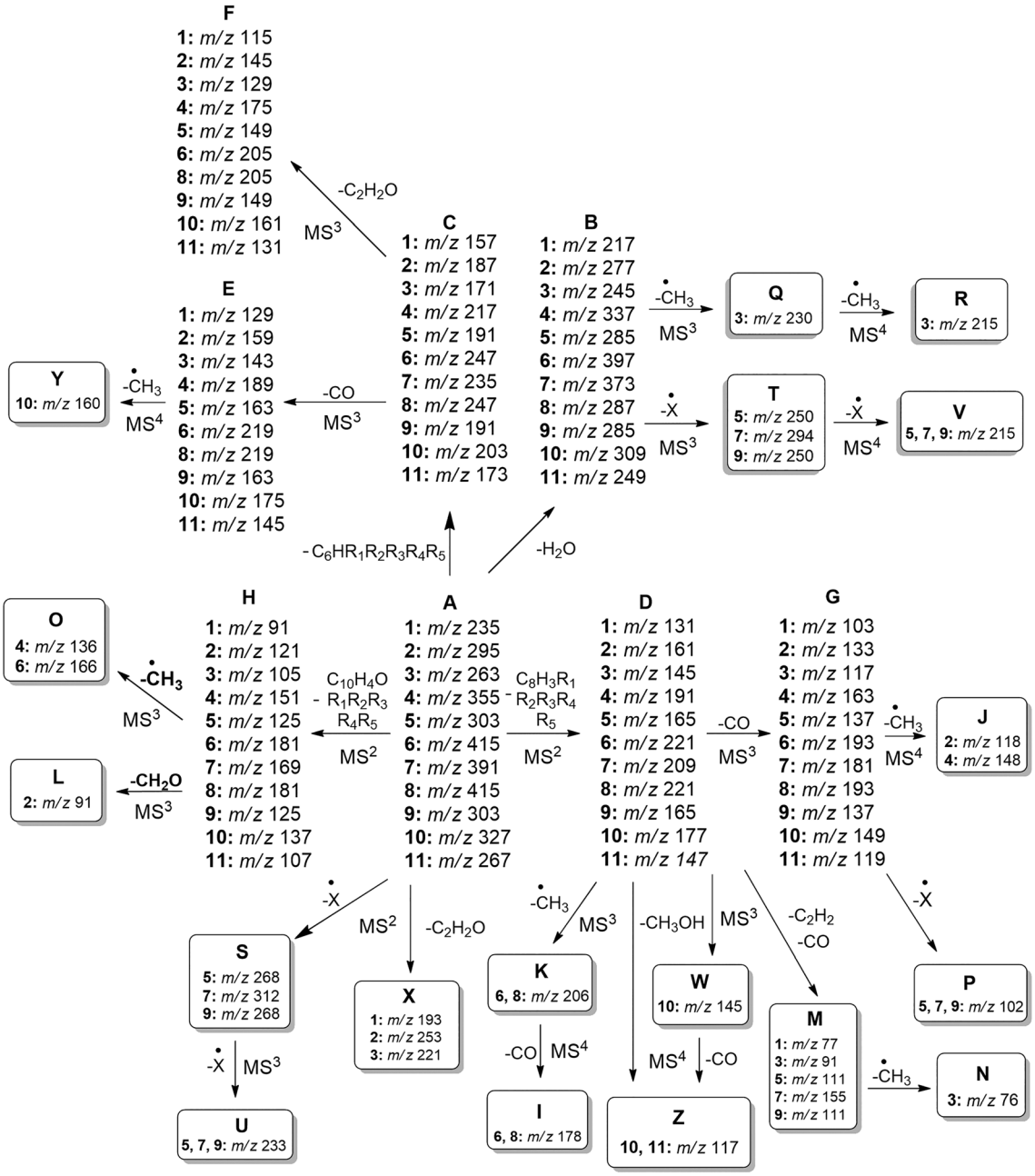

SCHEME 2 Structure–fragmentation correlations in protonated MKCs **1–11**

D (path II, Scheme 3) by means of a hydrogen rearrangement is similar to the hydrogen rearrangement that has been previously reported for 2-aroylbenzofurans[15] and chalcones.[25] This mechanism is fully supported by data from the deuterium-exchange experiments (Table 1). For compounds **1** and **2**, the **D** structure has been proposed.[11] Experimental data revealed that **H** is more intense than D in the product ion spectra of compounds **1–3**, **5**, **7**, and **9–11**, whereas **D** is more intense than **H** in the product ion spectra of compounds **4, 6**, and **8** at E_{lab} = 20 eV. ΔH values for **H** and **D** formation from **A** revealed that **A'** formation (which leads to **H** formation) is energetically more favored (–3.2–5.5 kcal.mol^{-1}) than **D** formation (ΔH values = 31.1–38.5 kcal.mol^{-1}, Scheme 3). Consequently, most of the precursor ions **A** are converted into **A'** instead of **D**, which could be explained by the higher intensity of **H** than that of **D**. **D** is further converted into **G** by elimination of CO resulting from heterolytic C1–C2 bond cleavage. However, our calculations revealed that the vinylic ion **G** is unstable (it spontaneously rearranged to **G1** during the geometry optimization). The calculated ΔH values indicated that the **D** → **G1** conversion is less favored for compounds **4** (ΔH = 50.5 kcal.mol^{-1}), **6** (ΔH = 51.0 kcal.mol^{-1}), and **8** (ΔH = 38.6 kcal.mol^{-1}) than for the other MKCs. This can be related to the presence of more than one methoxyl group at the aromatic rings, which stabilizes the **D** structure compared with **G1** due to their electron-release mesomeric effect.

Because of the higher stability of **D** derived from compounds **4**, **6**, and **8**, a reduced number of **D** ions are converted into **G/G1**, so that a high number of intact ions **D** reach the detector. This can explain, at least in principle, why **D** is the base peak in the product ion spectra of compounds **4**, **6**, and **8** (Table 1).

For compounds **2**, **3**, **5**, **7**, and **9**, the nature of the substituent at the aromatic ring also plays an essential role in formation of **G** from **D** (Scheme 4). For compounds **2** and **3**, which bear a methyl and a methoxy substituent at the aromatic ring *p*-position, respectively, the relative intensity of **G** is higher than 70%. On the other hand, for compounds **5**, **7**, and **9**, which have a halogen (F or Cl) attached to the aromatic ring, the **G/G1** intensity is lower than 35%. These relative intensities are consistent with the estimated ΔH values for the **D** → **G/G1** decomposition; these values are lower for compounds **2** (ΔH = 27.1 kcal.mol^{-1}) and **3** (ΔH = 29.2 kcal.mol^{-1}) than for compounds **5** (ΔH = 30.7 kcal.mol^{-1}), **7** (ΔH = 30.2 kcal.mol^{-1}), and **9** (ΔH = 30.1 kcal.mol^{-1}). This increase in the relative intensity of **G** in compounds **2** and **3** compared with compounds **5**, **7**, and **9** can be due to the methyl group hyperconjugative effect in compound **3** and to the methoxy group electron-release mesomeric effect in compound **2**, which contribute to stabilizing the vinylic cation **G1**.

Nazarov cyclization in protonated curcuminoids has been reported to occur in solution and in the gas phase.[11] Cyriac and co-workers established that ketene and arene losses from the protonated MKCs 1,5-*bis*-(2-methoxyphenyl)-1,4-pentadien-3-one and 1,5-*bis*-(2-hydroxyphenyl)-1,4-pentadien-3-one are preceded by Nazarov cyclization and further aryl migration. The authors proposed some possible transition states (TSs) involved in [MKC + H–arene]$^+$ and [MKC + H–ketene]$^+$ formation and supported their hypothesis by ΔH values estimated by computational calculations. The authors concluded that the oxygen atom (a hydroxyl or a methoxyl group at C9 and C9') plays a crucial part in these steps. They also reported losses of arene and ketene for compounds **1** and **2**; however, they postulated that these processes must involve different fragmentation pathways without providing further details. Here, we provide an alternative mechanism for [MKC + H – arene]$^+$ and [MKC + H – ketene]$^+$ formation that operates for various compounds and which does not depend on the presence of the oxygen atom at the aromatic ring.

For compounds **1–9**, Nazarov cyclization involves the most stable conformer **A1** and produces **A1'** (pathway III, Scheme 4). Water elimination from **A1** to produce **B** is preceded by aryl migration from C3 to C2 and consequent **A1"** formation. The aryl migration mechanism has been extensively investigated by Cyriac and co-workers.[11] Nevertheless, although the authors reported water elimination from protonated **1** and **2**, they did not discuss the underlying mechanisms or the ion structures. **B** (**A1**–H_2O) and **C** (**A1**–$C_6HR_1R_2R_3R_4R_5$), which are stabilized by resonance, are competitively formed from **A1'**. However, the peak corresponding to **C** is more intense than that corresponding to **B** in the product ion spectra of protonated MKCs **1–9**. This difference between the intensities of **B** and **C** can be interpreted in terms of the ΔH values estimated for pathways IIIa and IIIb, which revealed that formation of **C** from **A1'** (pathway IIIa, ΔH between −8.2 and 5.6 kcal.mol^{-1}) is energetically more favored than formation of **A1"** (pathway IIIb, ΔH between 0.0 to 5.2 kcal.mol^{-1}) for all the analyzed MKCs.

For MKCs **1–9**, **E** and **F** originate from **C**, as evidenced by the MS^3 experiments (see supporting information). **E** and **F** result from

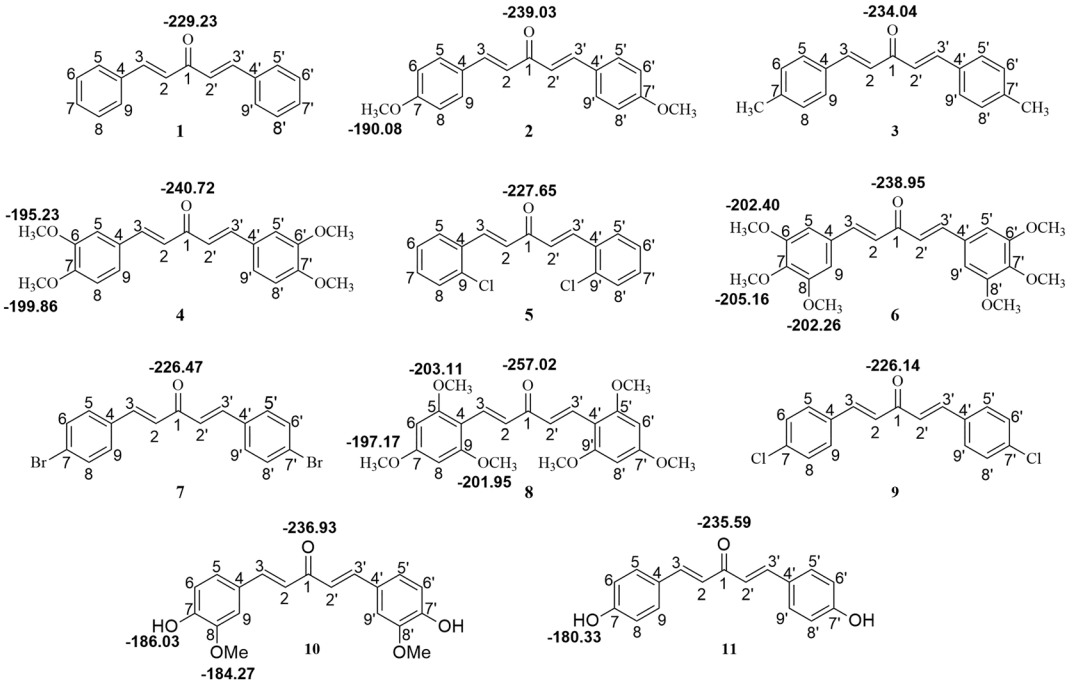

FIGURE 4 Proton affinity (PA) values for monoketone curcuminoides **1–11**. The PA values were calculated at the B3LYP/6-31+G(d,p) level. All the PA values are in kcal.mol^{-1}

two competitive ring contractions of cyclic ketone **C1** (the most stable tautomer in the equilibrium with **C**), which lead to elimination of CO (28 Da) and ketene (42 Da), respectively.[25] **F** has an unstable structure and is spontaneously converted into **F1** during geometry optimization. The estimated ΔH and ΔG values for **C1** conversion into **E** and **F1** are 25.9–30.7 kcal.mol^{-1} and 14.5–19.2 kcal.mol^{-1} for **E** and 50.1–58.2 kcal.mol^{-1} and 33.6–43.6 kcal.mol^{-1} for **F1**, respectively. These values fully agree with the experimental results, as the intensity of **E** is greater than the intensity of **F** at E_{lab} = 20 eV. In the case of compound **7**, ions **E** and **F** do not apear in the product ion spectrum. A possible explanation for this is that formation of **C**, which leads to formation of **E** (ΔH = 28.67 kcal.mol^{-1}) and

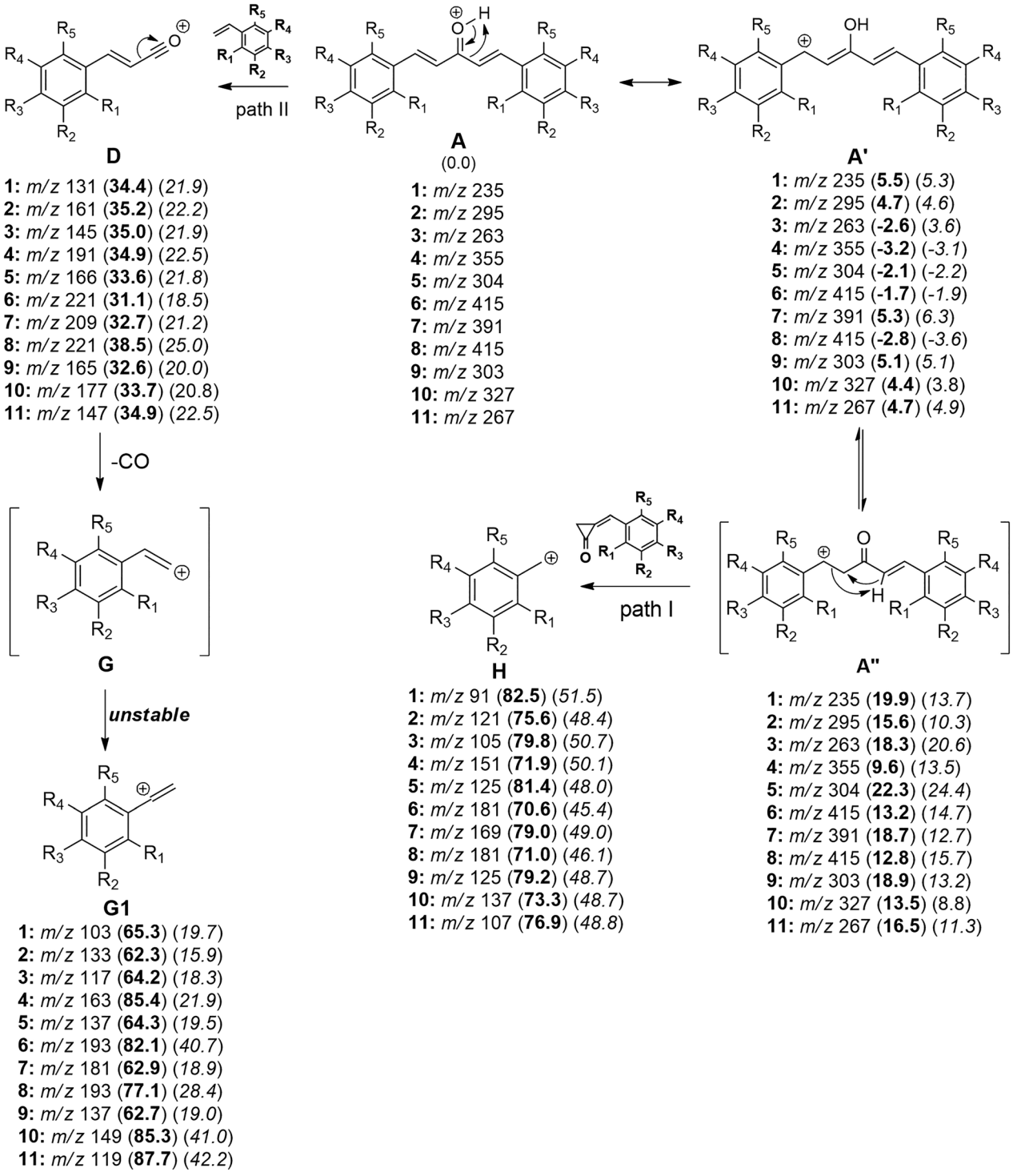

SCHEME 3 Formation of product ions **D**, **G**, and **H** from protonated MKCs **1–11**. Relative **enthalpies** (ΔH) and *Gibbs energies* (ΔG) values are in kcal.mol^{-1}

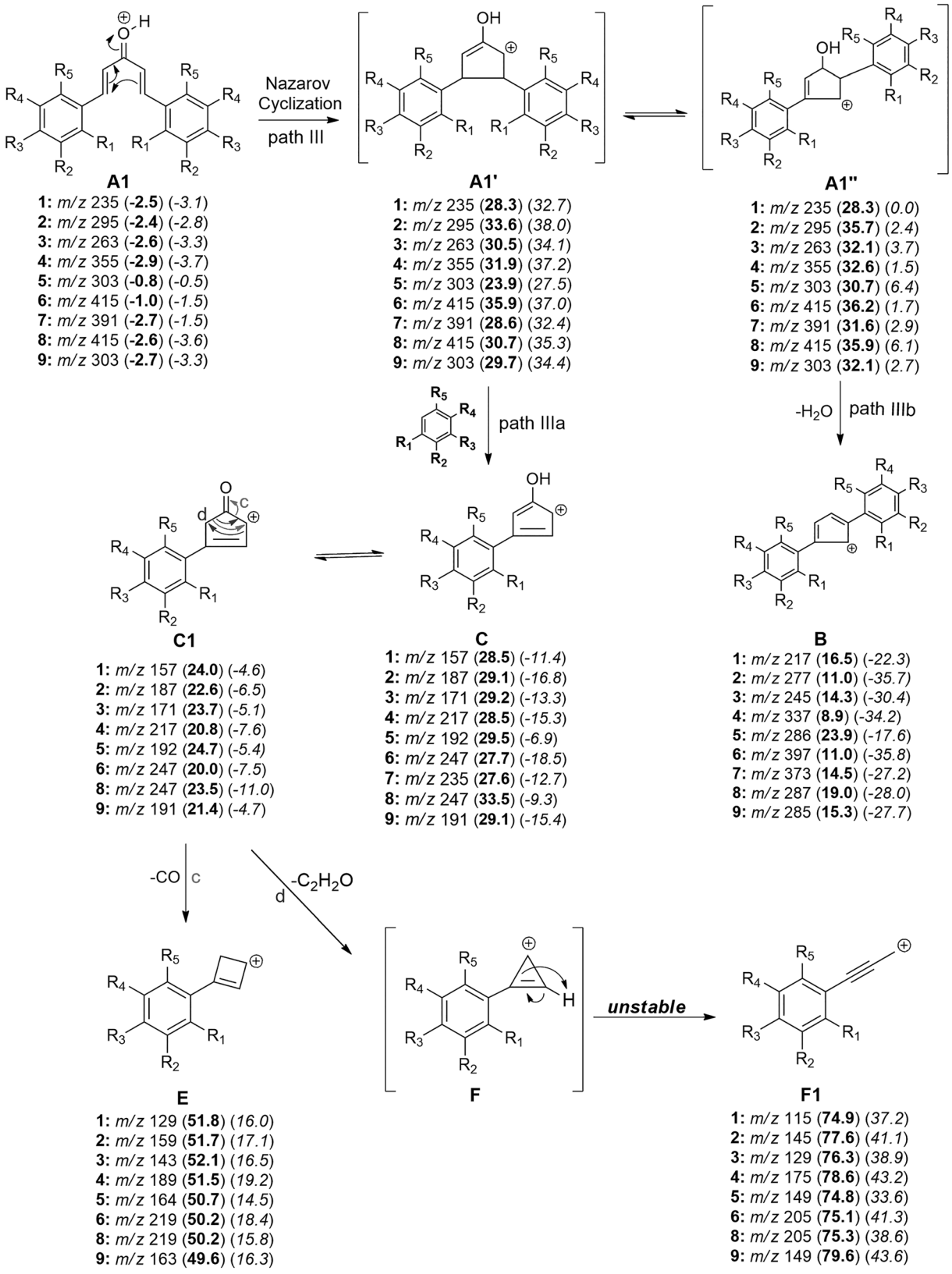

SCHEME 4 Formation of product ions **B**, **C**, **E**, and **F** from protonated MKCs **1–9**. Relative **enthalpies** (ΔH) and *Gibbs energies* (ΔG) values are in kcal.mol^{-1}

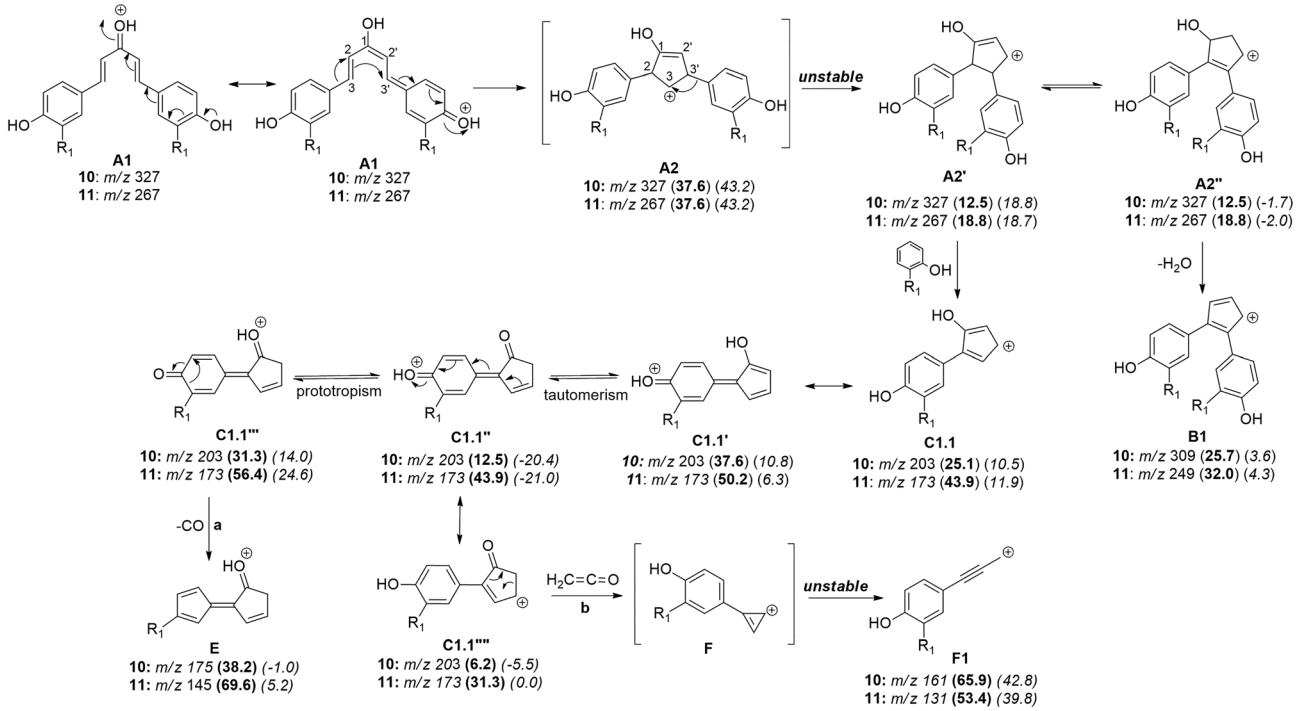

SCHEME 5 Formation of product ions **B**, **C**, **E**, and **F** from compounds **10** and **11**

F (ΔH = 58.35 kcal.mol^{-1}), competes with the formation of the diagnostics ions **S** and **U** (ΔH = 0.13 kcal.mol^{-1}), which are energetically more favored (Scheme 6). This result also agrees with the intensities in the product ion spectrum.

In the case of MKCs **10** and **11**, the expected cyclic structure resulting from Nazarov cyclization (**A1'**) is spontaneously converted into **A1** during geometry optimization. This led us to conclude that formation of **B**, **C**, **E**, and **F** for these compounds is due to a different fragmentation pathway from that in compounds **1–9**, as shown in Scheme 5. In these cases, cyclization is followed by an 1,2-aryl migration from C3 to C2 to produce **A2**. However, the **A2** structure is unstable and is spontaneously converted into **A2'** by means of a second 1,2-aryl migration from C3 to C3' (Scheme 5). The **A2'** structure has also been reported by Cyriac and co-workers to explain

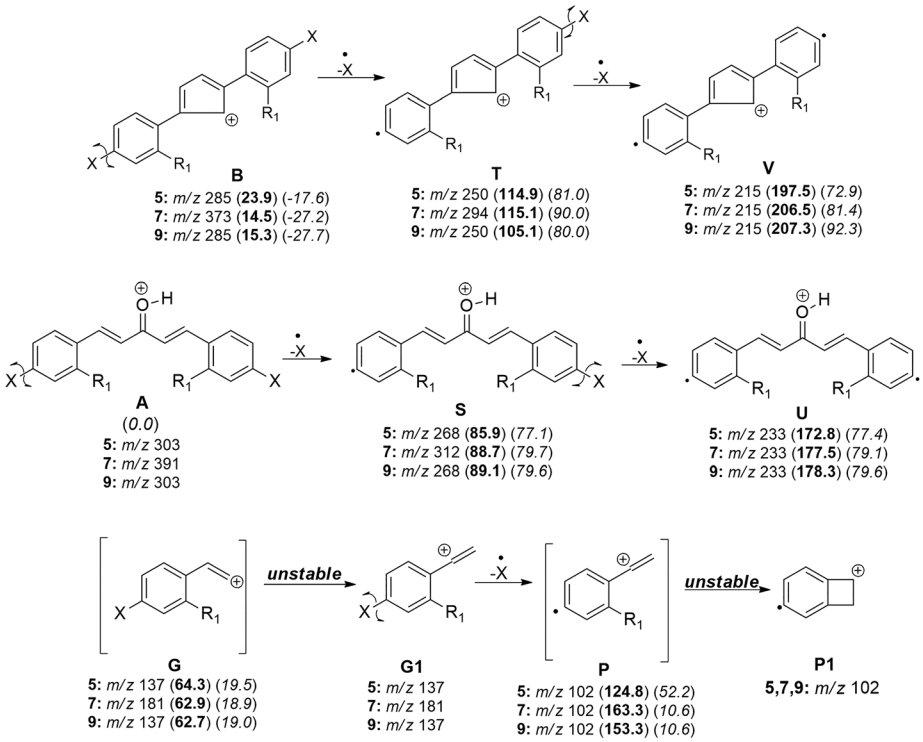

SCHEME 6 Formation of diagnostic product ions **P**, **S**, **T**, **U**, and **V** from compounds **5**, **7**, and **9**. Relative **enthalpies** (ΔH) and *Gibbs energies* (ΔG) values are in kcal.mol^{-1}

SCHEME 7 Formation of diagnostic product ions **Q** and **R** from compound **3**. Relative **enthalpies** (ΔH) and *Gibbs energies* (ΔG) values are in kcal.mol^{-1}

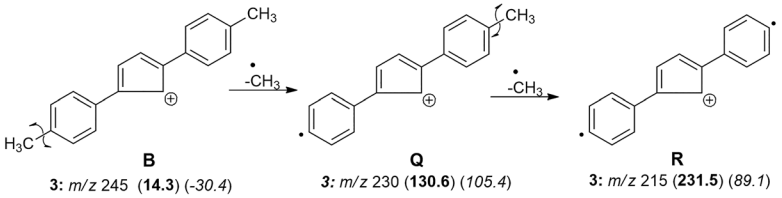

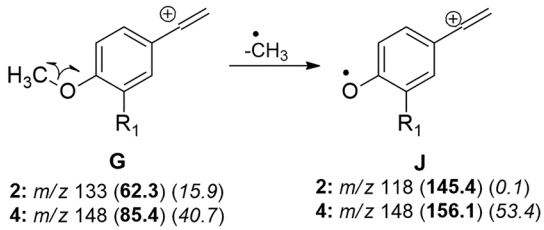

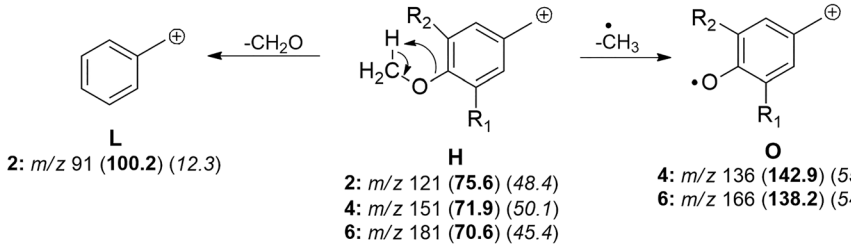

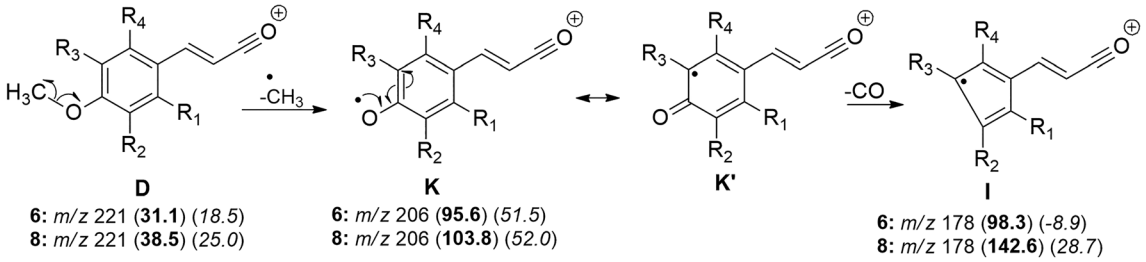

SCHEME 8 Formation of diagnostic product ions **J**, **L**, **O**, **K**, and **I**. Relative **enthalpies** (ΔH) and *Gibbs energies* (ΔG) values are in kcal.mol^{-1}

1,5-*bis*-(2-methoxyphenyl)-1,4-pentadien-3-one fragmentation.[11] Formation of **B1** ($[M + H - H_2O]^+$ is preceded by **A2'** isomerization into **A2"**, which is an energetically favored process (ΔH = 13.2 kcal.mol^{-1}, ΔG = 3.6–4.32 kcal.mol^{-1}). On the other hand, formation of **C**, **D**, **E**, and **F** involves arene elimination (Scheme 5). Formation of **C1.1** from **A2'** is energetically more favored for compound **10** (ΔH = 12.6 kcal.mol^{-1}) than for compound **11** (ΔH = 25.1 kcal.mol^{-1}). Consequently, peaks corresponding to **E** and **F**, which are derived from **C**, are more intense in the product ion spectrum of compound **10** than in that of compound **11** (Table 1).

Cyriac and co-workers suggested that Nazarov cyclization and subsequent arene and ketene losses from protonated MKC **2** and 1,5-*bis*-(2-hydroxyphenyl)-1,4-pentadien-3-one occur. The latter compounds bear methoxyl and hydroxyl groups at the *para* (C8 and C7) and *ortho* positions, respectively.[11] Because the CID energy that is necessary to dissociate compound **2** is higher than that required to fragment its *ortho* isomer, the authors proposed that the mechanisms involved in the Nazarov cyclization of these two compounds differ and depend on the position of the methoxy group. Here, we revisit the MKC **2** fragmentation and investigate the fragmentation of

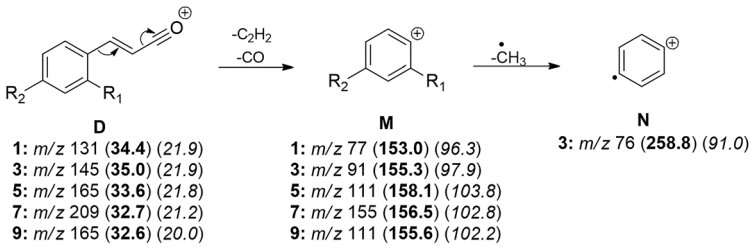

SCHEME 9 Formation of diagnostic product ions **M** from protonated MKCs **1**, **3**, **5**, **7**, and **9** and **N** from compound **3.** Relative **enthalpies** (ΔH) and *Gibbs energies* (ΔG) values are in kcal.mol^{-1}

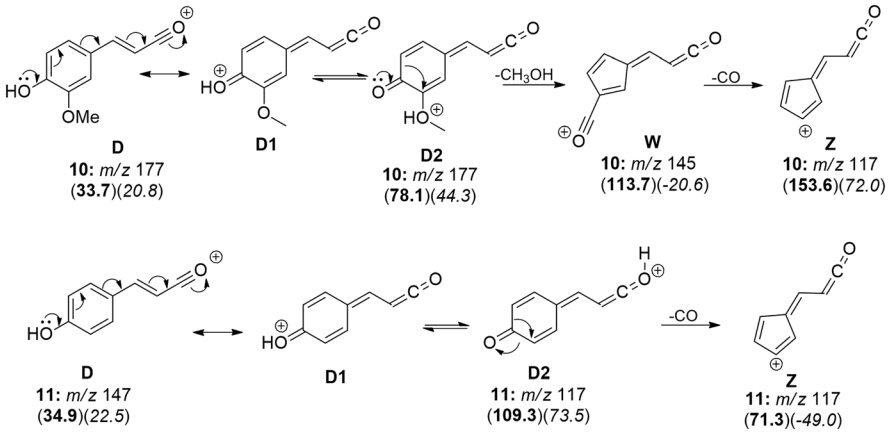

SCHEME 10 Formation of diagnostic product ions **W** from compound **10** and **Z** from compounds **10** and **11**

compound **11**, which is the *para* isomer of 1,5-*bis*-(2-hydroxyphenyl)-1,4-pentadien-3-one. Our results indicated that Nazarov cyclization and subsequent ketene and arene losses from protonated **2** follow the same fragmentation pathway as in compounds **1** and **3–9**, thus revealing that formation of **B**, **C**, **E**, and **F** does not depend on the presence of an oxygen atom at the *ortho* position of the aromatic ring. In contrast, calculations carried out at the B3LYP level of theory demonstrated that the **A1'** ion structure of compounds **10** and **11**, which display a hydroxyl group at the *para* position, is spontaneously converted back into **A1**. This implies that, compared with compounds **1–9**, formation of **B**, **C**, **E**, and **F** follows a different fragmentation pathway in the case of compounds **10** and **11**. On the other hand, our theoretical calculations revealed that the **A1'** structure corresponding to 1,5-*bis*-(2-hydroxyphenyl)-1,4-pentadien-3-one, which displays a hydroxyl group at the *ortho* position, is stable and is not converted back into **A1**. These data evidenced that the position of the hydroxyl group plays a key part in the fragmentation of MKCs. However, the hydroxyl effect on the mechanism appears to be more related to the formation of an intramolecular hydrogen bond than to the hydroxyl hydrogen, as was previously suggested by Cyriac and co-workers.[11] In the case of 1,5-*bis*-(2-hydroxyphenyl)-1,4-pentadien-3-one, the intramolecular hydrogen bond between the two hydroxyl groups at the *ortho* position stabilizes the **A1'** structure resulting from Nazarov cyclization, so that its fragmentation is similar for MKCs **1–9**. In the case of compounds **10** and **11**, this stabilizing interaction does not occur – the hydroxyl group is now involved in an intramolecular hydrogen bond with the methoxyl group at the adjacent carbon, which causes **A1'** to be converted back into **A1**.

3.4 | Formation of diagnostic ions

Product ions produced by homolytic C–X bond cleavage (X = Cl or Br) and consequent X• elimination are diagnostic for the presence of Cl and Br in the structures of compounds **5**, **7**, and **9**. Schemes 2 and 6 illustrate formation of **T** from **B**, formation of **V** (*m/z* 215) from **T**, and formation of **P** (*m/z* 102) from **G**. The ΔH values estimated for the conversion of **B** into **T** for compounds **5**, **7**, and **9** are 90.7, 100.6, and 86.1 kcal.mol^{-1}, respectively. Formation of **S** (*m/z* 268 and *m/z* 312) from **A**, formation of **U** (*m/z* 233) from **S**, and formation of **P** from **G** occur through a similar mechanism (Scheme 6). The ΔH values involved in formation of **U** are 86.9, 88.8, and 89.2 kcal.mol^{-1} for compounds **5**, **7**, and **9**, respectively. The ΔH values for formation of **P** are 60.5, 100.4, and 90.6 kcal.mol^{-1} for compounds **5**, **7**, and **9**, respectively. However, formation of **P**, **S**, and **T** violates the even-electron rule, so it is disfavored by enthalpy.[27–29] On the other hand, formation of **V** and **U** from **T** and **S** agrees with the odd-electron rule. This could explain, at least in principle, the higher relative intensity of **V** and **U** than that of their precursors **T** and **S**. However, although formation of **U** and **V** is in accordance with the odd-electron rule, the ΔH values are still high because of the formation of bi-radicals. In the case of compound **7**, which has a bromine atom attached to the aromatic ring, the higher relative intensity of **S** and **U** than that of compounds **5** and **9** is probably due to the lower C–Br bond energy than that of C–Cl.

Q (*m/z* 230) and **R** (*m/z* 215) are also diagnostic for a methyl group at the aromatic ring for compound **3**. These ions originate from a mechanism that resembles that involved in **T** and **V**, as well as in **S** and **U** formation, as previously discussed in this paper (Scheme 7). The ΔH and ΔG values involved in formation of **Q** and **R** are 116.3 and 105.48 for **Q**, respectively, and 100.9 and 89.18 kcal.mol^{-1} for **R**, respectively. Formation of **J** (*m/z* 118) from **G** (compounds **2** and **4**), formation of **O** (*m/z* 136 and 166) from **H** (compounds **4** and **6**), and formation of **K** from **D** (compounds **6** and **8**) are diagnostic for the methoxy groups at the aromatic rings of MKCs **2**, **4**, **6**, and **8**, respectively. They originate from homolytic C10–O bond cleavage and consequent elimination of a methyl radical (Scheme 8).

For compounds **6** and **8**, CO elimination from the aromatic ring to produce **I** (*m/z* 178) involves a ring contraction that produces **K** and

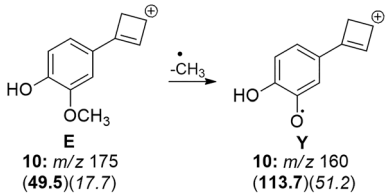

SCHEME 11 Formation of diagnostic ion **Y** from compound **10**

consequently expels CO from the phenoxyl radical ketone form (Scheme 8). Methyl radical eliminations followed by decarbonylation have been previously reported for many compounds displaying aromatic methoxy groups.[8,27] Elimination of the methyl radical from **D** to form **K** violates the even-electron rule.[27-29] and is energetically disfavored (ΔH = 95.6 kcal.mol^{-1} for compound **6** and 103.8 kcal.mol^{-1} for compound **8**) due to loss of aromaticity, which agrees with its relative intensity in the product ion spectra. On the other hand, formation of **L** (*m/z* 91) from **H**, which is diagnostic for the presence of a methoxy group at the aromatic ring of compound **2**, results from a remote hydrogen rearrangement and consequent elimination of CH_2O (30 Da), as shown in Scheme 8. The estimated ΔH and ΔG values for conversion of **H** into **L** are 24.6 and 12.3 kcal.mol^{-1}, respectively. For compounds **4**, **6**, and **8**, which bear more than one methoxy in the aromatic ring, CH_2O loss and consequent formation of **L** do not occur. This is probably due to the presence of more than one methoxy group at specific positions on the aromatic ring of these compounds, which tends to favor other pathways (e.g., **K** and **O** formations) in competition with formation of **L**.

Acetylene (C_2H_2) elimination concomitant to CO loss from **D** produces **M**, as shown in Scheme 9. Although no specific substituent participates in formation of **M**, this ion arises only for compounds **1**, **3**, **5**, **7**, and **9**. This is possibly because formation of **M** competes with formation of **G**. The ΔH values revealed that formation of **G** (ΔH = 27.1–52.8 kcal.mol^{-1}) is more energetically favored than formation of **M** (ΔH = 118.09–124.54 kcal.mol^{-1}). Conversion of **D** into **M** is more endothermic (ΔH = 118.6–124.5 kcal.mol^{-1}) and endergonic (ΔG = 96.3–103.8 kcal.mol^{-1}) than formation of **G** from **D**, which is consistent with the relative intensity of **M** in the product ion spectrum. In addition, for the other compounds, the substituents attached to the aromatic ring yield other product ions in competition with formation of **M**. For example, formation of **K** (*m/z* 206) from **D** is diagnostic for compounds **6** and **8**, while formation of **W** (*m/z* 145) for compound **10** and formation of **Z** (*m/z* 117) for compounds **10** and **11** compete with formation of **M** from **D**. Further methyl radical ($\bullet CH_3$) elimination from **M** produces the distonic ion (*m/z* 76), which is diagnostic for compound **3**. Although the low ΔH and ΔG values favor formation of **N** (ΔH = 103.5 kcal.mol^{-1} and ΔG = 91.0 kcal.mol^{-1}), its relatively low intensity in the product ion spectrum of curcuminoid **3** can be attributed to competition with the formation of diagnostic ions **Q** and **R**. In addition, **M** comes from **D**, whose formation from **A** is favored compared with formation of **H** only for compounds **4**, **6**, and **8**. Consequently, most of the product ions originating from **G** present low relative intensities in the product ion spectra (Table 1).

In the case of compound **10**, formation of diagnostic ions **W** (*m/z* 145) from **D** and **Z** (*m/z* 117) from **W** involves the hydroxyl group at C7, as shown in Scheme 10. For compound **10**, conversion of **D** into **W** (ΔH = 35.6 kcal.mol^{-1}) and conversion of **W** into **Z** are endothermic (ΔH = 39.9 kcal.mol^{-1}), which agrees with their relative low intensity in the product ion spectrum. For compound **11**, **Z** (*m/z* 117) is formed directly from **D**. However, the ΔH value involved in formation of **Z** from compound **11** is lower (ΔH = −38.0 kcal.mol^{-1}) than for the same ion in compound **10** (ΔH = 39.9 kcal.mol^{-1}). This difference may be associated with the difference between the structures of the D2 intermediates for the two compounds. On the other hand, product ion **Y**, which is diagnostic for compound **10**, originates from methyl radical removal from **D** (scheme 11). Formation of **Y** from **E** is disfavored by enthalpy (ΔH = 75.5 kcal.mol^{-1}), which agrees with the low intensity of **Y** in the product ion spectrum of compound **10**.

Finally, **X** results from direct ketene (42 Da) elimination from **A**. Formation of this product ion is preceded by conversion of **A1** into **A2**, which results from Nazarov cyclization, as shown in Scheme 12. As with formation of **B**, migration of an aryl from C3 to C2 consequently forms **A'''** (Scheme 12). The ΔH values revealed that formation of **X** is more energetically favored for compound **2** (ΔH = −16.0 kcal/mol^{-1}) than for compounds **1** (ΔH = 1.6 kcal/mol^{-1}) and **3** (ΔH = 2.3 kcal/mol^{-1}), which is consistent with the higher relative intensity of **X** in the product ion spectrum of compound **2** than in those of compounds **1** and **3**. In this case, **A2** is unstable and therefore rearranges spontaneously to **X** for the three compounds, as

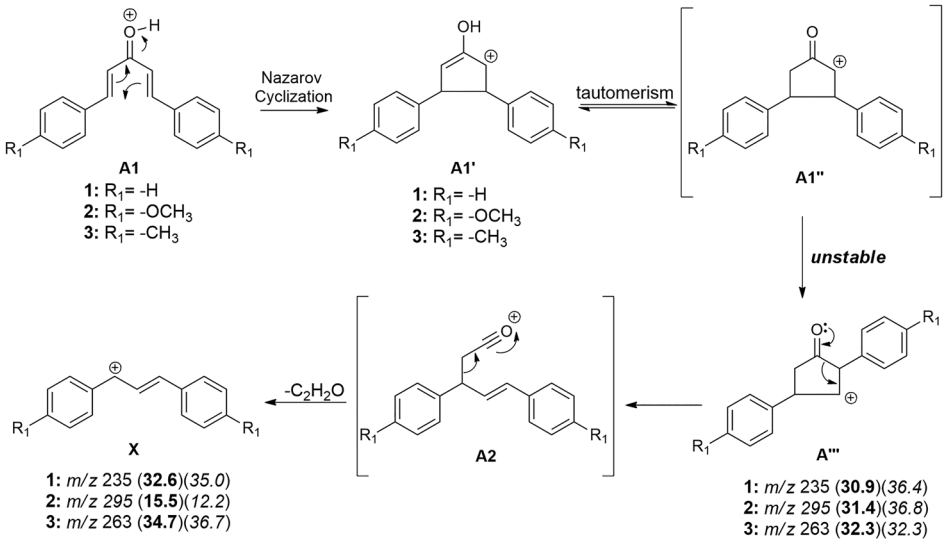

SCHEME 12 Formation of diagnostic product ion **X** from compounds **1**, **2**, and **3**. Relative **enthalpies** (ΔH) and *Gibbs energies* (ΔG) values are in kcal.mol^{-1}

can be seen in Scheme 12. For compounds **4**, **6**, and **8**, which display more than one methoxy group at the aromatic ring, the electron-releasing mesomeric effect of these groups further stabilizes **A'''** compared with the corresponding **A2** of the other compounds, thus increasing the energy barrier for its conversion into **X**. Consequently, **X** does not appear in the product ion spectra of compounds **4**, **6**, and **8** obtained at E_{lab} = 20 eV.

4 | CONCLUSIONS

Our results reinforce, at least in part, the fragmentation pathways previously reported in the literature. In addition, we propose an alternative fragmentation mechanism that can explain the fragmentation of a wider diversity of curcuminoids that do not display a hydroxyl group in their structures. The most intense product ions are acylium ions resulting from hydrogen rearrangement or product ions derived from Nazarov cyclization of the protonated molecule. The presence and the position of a hydroxyl group at the aromatic rings play a key role in the Nazarov cyclization mechanism. Thermochemical data estimated by computational chemistry helped to confirm the identity of the ion structures and to understand the experimental data, mainly with respect to the relative intensities of the peaks in the product ion spectra. These data, in combination with multiple-stage mass spectrometry (MS^n) and accurate mass data, can be further used to identify *in vitro* or *in vivo* metabolites obtained from curcuminoids in biological samples by LC/ESI-MS/MS.

ACKNOWLEDGEMENTS

The authors acknowledge grant numbers 2016/19272-9, 2011/07623-8, and 2017/24856-2 provided by the Fundação de Amparo à Pesquisa do Estado de São Paulo (FAPESP). This study was partially financed by Coordenação de Aperfeiçoamento de Pessoal de Nível Superior - Brasil (CAPES) - Finance Code 001. RLTP thanks the Conselho Nacional de Desenvolvimento Científico e Tecnológico (CNPq, Brazil, grant 313648/2018-2) for a research fellowship.

ORCID

Tatiana M. Vieira https://orcid.org/0000-0002-9469-8053
Renato P. Orenha https://orcid.org/0000-0001-7285-8098
Eduardo J. Crevelin https://orcid.org/0000-0001-8708-147X
Ricardo Vessecchi https://orcid.org/0000-0001-8472-3190
Renato L.T. Parreira https://orcid.org/0000-0002-5623-9833
Antônio E.M. Crotti https://orcid.org/0000-0002-1730-1729

REFERENCES

1. Liang G, Li X, Chen L, et al. Synthesis and anti-inflammatory activities of mono-carbonyl analogues of curcumin. *Bioorg Med Chem Lett*. 2008;18(4):1525-1529. https://doi.org/10.1016/j.bmcl.2007.12.068
2. Zamrus SNH, Akhtar MN, Yeap SK, et al. Design, synthesis and cytotoxic effects of curcuminoids on HeLa, K562, MCF-7 and MDA-MB-231 cancer cell lines. *Chem Cent J*. 2018;12(1):1-10. https://doi.org/10.1186/s13065-018-0398-1
3. Park SJ, Garcia CV, Shin GH, Kim JT. Improvement of curcuminoid bioaccessibility from turmeric by a nanostructured lipid carrier system. *Food Chem*. 2018;12:25151-25157. https://doi.org/10.1016/j.foodchem.2018.01.071
4. Vieira TM, Santos IA, Silva TS, Martins CHG, Crotti AEM. Antimicrobial activity of monoketone curcuminoids against cariogenic bacteria. *Chem Biodivers*. 2018;15(8):5-12. https://doi.org/10.1002/cbdv.201800216
5. Ud Din Z, Fill TP, de Assis FF, et al. Unsymmetrical 1,5-diaryl-3-oxo-1,4-pentadienyls and their evaluation as antiparasitic agents. *Bioorg Med Chem*. 2013;22(3):1121-1127. https://doi.org/10.1016/j.bmc.2013.12.020
6. Kumari N, Kulkarni A, Lin X, et al. Inhibition of HIV-1 by curcumin a, a novel curcumin analog. *Drug des Devel Ther*. 2015;2015(9):5051-5060. https://doi.org/10.2147/DDDT.S86558
7. Carrão DB, Albuquerque NCP, Marques LMM, et al. *In vitro* metabolism of artepillin C by rat and human liver microsomes. *Planta Med*. 2017;83(8):737-745. https://doi.org/10.1055/s-0042-124359
8. Demarque DP, Crotti AEM, Vessecchi R, Lopes JL, Lopes NP. Fragmentation reactions using electrospray ionization mass spectrometry: An important tool for the structural elucidation and characterization of synthetic and natural products. *Nat Prod Rep*. 2016;33(3):432-455. https://doi.org/10.1039/c5np00073d
9. Jiang H, Somogyi Á, Jacobsen NE, Timmermann BN, Gang DR. Analysis of curcuminoids by positive and negative electrospray ionization and tandem mass spectrometry. *Rapid Commun Mass Spectrom*. 2006;20(6):1001-1012. https://doi.org/10.1002/rcm.2401
10. Ostrowski W, Sniecikowska L, Hoffmann M, Franski R. Demethoxycurcumin-metal complexes: Fragmentation and comparison, with curcumin-metal complexes, as studied by ESI-MS/MS. *J Spectros*. 2013;2913(8): 1-8. https://doi.org/10.1155/2013/749641
11. Cyriac J, Paulose J, George M, et al. The role of methoxy group in the Nazarov cyclization of 1,5-*bis*-(2-methoxyphenyl)-1,4-pentadien-3-one in the gas phase and condensed phase. *J Am Soc Mass Spectrom*. 2014;25(3):398-409. https://doi.org/10.1007/s13361-013-0785-8
12. George M, Sebastian VS, Reddy PN, Srinivas R, Giblin D, Gross ML. Gas-phase Nazarov cyclization of protonated 2-methoxy and 2-hydroxychalcone: An example of intramolecular proton-transport catalysis. *J Am Soc Mass Spectrom*. 2009;20(5):805-818. https://doi.org/10.1016/j.jasms.2008.12.017
13. Crotti AEM, Bronze-Uhle ES, Nascimento PG, et al. Gas-phase fragmentation of gamma-lactone derivatives by electrospray ionization tandem mass spectrometry. *J Mass Spectrom*. 2009;44(12):1733-1741. https://doi.org/10.1002/jms.1682
14. Dias HJ, Baguenard M, Crevelin EJ, et al. Gas-phase fragmentation reactions of protonated benzofuran- and dihydrobenzofuran-type neolignans investigated by accurate-mass electrospray ionization tandem mass spectrometry. *J Mass Spectrom*. 2018;54(1):35-46. https://doi.org/10.1002/jms.4304
15. Dias HJ, Vieira TM, Crevelin EJ, Donate PM, Crotti AEM. Fragmentation of 2-aroylbenzofuran derivatives by electrospray ionization tandem mass spectrometry. *J Mass Spectrom*. 2017;52(12):809-816. https://doi.org/10.1002/jms.4024
16. Aguiar GP, Crevelin EJ, Dias HJ, et al. Electrospray ionization tandem mass spectrometry of labdane-type acid diterpenes. *J Mass Spectrom*. 2018;53(11):1086-1096. https://doi.org/10.1002/jms.4284
17. Dias HJ, Bento MVB, da Silva EH, et al. Gas-phase fragmentation reactions of protonated cocaine: New details to an old story. *J Mass Spectrom*. 2018;53(3):203-213. https://doi.org/10.1002/jms.4053
18. Dias HJ, Stefani R, Tomaz JC, Vessecchi R, Crotti AEM. Differentiation between 3,4- and 4,15-epoxyeudesmanolides by

electrospray ionization tandem mass spectrometry. *J Anal Methods Chem*. 2017;2017: 1-9. https://doi.org/10.1155/2017/7921867

19. Aguiar GP, Wakabayashi KAL, Luz GF, et al. Fragmentation of plumeran indole alkaloids from *Aspidosperma spruceanum* by electrospray ionization tandem mass spectrometry. *Rapid Commun Mass Spectrom*. 2010;24(3):295-308. https://doi.org/10.1002/rcm.4389
20. Vessecchi R, Carollo CA, Lopes JNC, Crotti AEM, Lopes NP, Galembeck SE. Gas-phase dissociation of 1,4-naphthoquinone derivative anions by electrospray ionization tandem mass spectrometry. *J Mass Spectrom*. 2009;44(8):1224-1233. https://doi.org/10.1002/jms.1600
21. Crevelin EJ, Possato B, Lopes JLC, Lopes NP. Precursor ion scan mode-based strategy for fast screening of polyether ionophores by copper-induced gas-phase radical fragmentation reactions. *Anal Chem*. 2017;89(7):3929-3936. https://doi.org/10.1021/acs.analchem.6b02855
22. Bouchoux G. Gas-phase basicities of polyfunctional molecules. Part 1: Theory and methods. *Mass Spectrom Rev*. 2007;26(6):775-835. https://doi.org/10.1002/mas.20151
23. Range K, Riccardi D, Cui Q, Elstner M, York DM. Benchmark calculations of proton affinities and gas-phase basicities of molecules important in the study of biological phosphoryl transfer. *Phys Chem Chem Phys*. 2005;7(16):3070-3079. https://doi.org/10.1039/b504941e
24. Boyd R, Somogyi Á. The mobile proton hypothesis in fragmentation of protonated peptides: A perspective. *J Am Soc Mass Spectrom*. 2010;21(8):1275-1278. https://doi.org/10.1016/j.jasms.2010.04.017
25. Hu N, Tu YP, Liu Y, Jiang K, Pan Y. Dissociative protonation and proton transfers: Fragmentation of α,β-unsaturated aromatic ketones in mass spectrometry. *J Org Chem*. 2008;73(9):3369-3376. https://doi.org/10.1021/jo702464b
26. Sleno L, Volmer DA. Ion activation methods for tandem mass spectrometry. *J Mass Spectrom*. 2004;39(10):1091-1112. https://doi.org/10.1002/jms.703
27. Karni MA. The "even-electron rule". *Org Mass Spectrom*. 1980;15(2):53-64. https://doi.org/10.1002/oms.1210150202
28. McLafferty FW, Turecek F. *Interpretation of Mass Spectra*. 4th ed. Sausalito: University Science Books; 1993.
29. Schäfer M, Dray M, Springer A, Zacharias P, Meerholz K. Radical cations in electrospray mass spectrometry: Formation of open-shell species, examination of the fragmentation behavior in ESI-MS^n and reaction mechanism studies by detection of transient radical cations. *Eur J Org Chem*. 2007;2007:5162-5174. https://doi.org/10.1002/ejoc.20070019

SUPPORTING INFORMATION

Additional supporting information may be found online in the Supporting Information section at the end of this article.

How to cite this article: Vieira TM, Orenha RP, Crevelin EJ, et al. Electrospray ionization tandem mass spectrometry of monoketone curcuminoids. *Rapid Commun Mass Spectrom*. 2020;e8699. https://doi.org/10.1002/rcm.8699